

ECHO FLOW NETWORKS

Hongbo Liu* Jia Xu *

Gateway Academic Center, Stevens Institute of Technology

601 Hudson St, Hoboken, NJ 07030

hliu93@stevens.edu, jxu70@stevens.edu

ABSTRACT

At the heart of time-series forecasting (TSF) lies a fundamental challenge: how can models efficiently and effectively capture long-range temporal dependencies across ever-growing sequences? While deep learning has brought notable progress, conventional architectures often face a trade-off between computational complexity and their ability to retain accumulative information over extended horizons.

Echo State Networks (ESNs), a class of reservoir computing models, have recently regained attention for their exceptional efficiency, offering constant memory usage and per-step training complexity regardless of input length. This makes them particularly attractive for modeling extremely long-term event history in TSF. However, traditional ESNs fall short of state-of-the-art performance due to their limited nonlinear capacity, which constrains both their expressiveness and stability.

We introduce **ECHO FLOW NETWORKS (EFNs)**, a framework composed of a group of extended Echo State Networks (**X-ESNs**) with MLP readouts, enhanced by our novel Matrix-Gated Composite Random Activation (**MCRA**), which enables complex, neuron-specific temporal dynamics, significantly expanding the network’s representational capacity without compromising computational efficiency. In addition, we propose a dual-stream architecture in which recent input history dynamically selects signature reservoir features from an infinite-horizon memory, leading to improved prediction accuracy and long-term stability.

Extensive evaluations on five benchmarks demonstrate that **EFNs** achieves up to 4 \times faster training and 3 \times smaller model size compared to leading methods like PatchTST, reducing forecasting error from 43% to 35%, a 20% relative improvement. One instantiation of our framework, **EchoFormer**, consistently achieves new state-of-the-art performance across five benchmark datasets: ETTh, ETTm, DMV, Weather, and Air Quality.

1 INTRODUCTION

Time-series forecasting (TSF) is a fundamental problem at the core of scientific discovery and decision-making, powering critical applications in climate science, finance, healthcare, and energy systems by predicting future trends from historical data. A key challenge in TSF is modeling *long-range temporal dependencies*, where the effects of past events unfold gradually. For instance, seasonal droughts can influence wildfire risk months later, and early market signals may foreshadow shifts in cryptocurrency prices (Chen et al., 2023; Ma et al., 2024).

While capturing long-range dependencies, and ideally learning from the entire history of inputs, is essential for accurate prediction, fully leveraging such historical context remains an open challenge due to two critical limitations. First, **computational inefficiency**: Transformer-based models like PatchTST (Nie et al., 2023) exhibit quadratic complexity in time and memory (Vaswani et al., 2017), making them impractical for ultra-long sequences. Even with recent efficiency improvements (Jia et al., 2024; Lin et al., 2023; Chi, 2024), these models still rely on backpropagation through time, resulting in high training cost and limited scalability. Second, **model limitations**: many models struggle with vanishing gradients and suffer from bifurcation issues, leaving significant room for performance improvement using long history (Lim & Zohren, 2021; Zhou et al., 2021; Nie et al., 2023). (Lim & Zohren, 2021; Zhou et al., 2021; Nie et al., 2023).

*Authors are listed in alphabetical order.

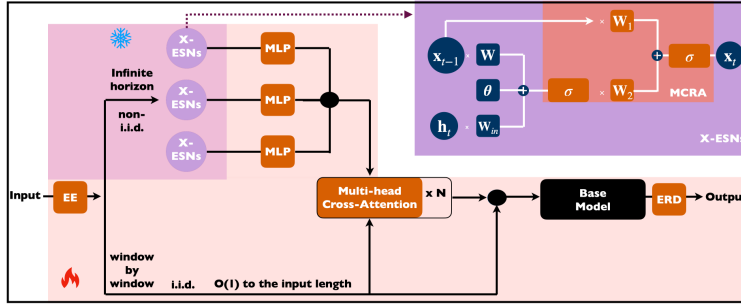


Figure 1: **EFNs** Framework with X-ESNs, and **MCRA** ($\mathbf{W}_1, \mathbf{W}_2, \sigma$).

Echo State Networks (ESNs) (Jaeger, 2001; Lukoševičius & Jaeger, 2009), as a kind of reservoir computing, offer a promising yet underexplored alternative. ESNs are lightweight autoregressive models with **linear time** and **constant space complexity**. Unlike attention-based models that truncate historical inputs or RNNs that compress past information into fixed-size hidden states, ESNs update their internal dynamics in a streaming fashion using randomly initialized, fixed weights, **without backpropagation**. This design enables a constant $\mathcal{O}(1)$ training cost per time step and a constant $\mathcal{O}(1)$ memory footprint, as well as an overall training time complexity of $\mathcal{O}(N)$. Furthermore, the reservoir acts as a denoising temporal encoder that is robust to bifurcations and gradient decay (Bollt, 2021; Vlachas et al., 2020), making ESNs ideal for modeling long-sequence patterns.

Yet, despite their theoretical advantages, ESNs have historically underperformed on time-series forecasting (TSF) tasks and, as a result, are not widely adopted. In this work, we identify three core limitations contributing to this underperformance and propose solutions to overcome them. First, ESNs suffer from **limited expressiveness in both state updates and readouts**. Classical ESNs typically employ a single nonlinearity (e.g., \tanh) in the state update and a linear readout layer, restricting their ability to capture complex temporal dynamics. This limitation is especially pronounced when the reservoir is too small or poorly aligned with task-relevant features, leading to failures in modeling hierarchical, compositional, or multi-scale structures that are challenging to decode linearly. Second, ESNs are **highly sensitive to random initialization**: since reservoir weights are fixed and randomly assigned rather than learned, performance can vary significantly between runs, often necessitating heuristic tuning or task-specific adjustments for stability (Rodan & Tiño, 2011; Lu et al., 2017). Third, ESNs **lack a dynamic, token-specific weighting mechanism**, such as attention, which hinders their ability to selectively focus on informative inputs, adapt to abrupt temporal shifts, or model non-smooth and discrete patterns. Together, these limitations constrain the ability of ESNs to achieve state-of-the-art performance.

In this paper, we propose **EFNs (ECHO FLOW NETWORKS)**, a novel framework that combines the efficiency of classical Echo State Networks (ESNs) with the expressive power of modern deep sequential models. **EFNs** enhances ESNs with spiking dynamics, grouped Extended ESNs (X-ESNs), and a dual-stream fusion mechanism for expressiveness, stability, and near token dependency.

As illustrated in Figure 1, **EFNs** consists of two main components integrated via masked multi-head attention: a recent input encoder operating over the k -length short-term window, and a **grouped X-ESN** that captures dynamics from the entire input history. **EFNs** can function as a standalone forecasting model or be used to boost existing TSF methods in a black-box manner. Specifically, our approach introduces four key innovations:

1. **X-ESNs with MCRA for Expressiveness:** Extended ESNs (**X-ESNs**) augment traditional Echo State Networks (ESNs) with our proposed Matrix-Gated Composite Random Activation (**MCRA**). Unlike the standard single \tanh activation, **MCRA** employs a composition of two nonlinear activation functions to jointly transform the current input and the previous state, enabling the modeling of more complex temporal structures. Each activation function is randomly selected from a predefined set (e.g., ReLU, Leaky ReLU, \tanh , and **Sigmoid**), increasing functional diversity within the ensemble mechanism of **Group X-ESNs** for improved accuracy and stability.

Furthermore, **MCRA** replaces the scalar leaky integration parameter with matrix-valued gates, allowing for more expressive and adaptable neuron-specific temporal dynamics.

The conventional ESNs, i.e., LI-ESN (Jaeger et al., 2007), evolves the reservoir state $\mathbf{x}_t \in \mathbb{R}^{N_r}$ as:

$$\mathbf{x}_t = (1 - \alpha)\mathbf{x}_{t-1} + \alpha \tanh(\mathbf{W}_{\text{in}}\mathbf{h}_t + \boldsymbol{\theta} + \mathbf{W}\mathbf{x}_{t-1}), \quad (1)$$

where $\mathbf{h}_t \in \mathbb{R}^{N_u}$ is the input at time t , \mathbf{W}_{in} , \mathbf{W} , and $\boldsymbol{\theta}$ are the input, recurrent, and bias parameters, respectively, and $\alpha \in [0, 1]$ is the leaky integration rate controlling memory decay. N_r and N_u are reservoir and input dimension, respectively. Weights are drawn from $\mathcal{U}[-\sigma_{\text{in}}, \sigma_{\text{in}}]$, and \mathbf{W} is scaled to satisfy the Echo State Property (ESP) (Tiňo et al., 2007) via the spectral radius condition.

We extend this formulation in **X-ESNs** by introducing the *Matrix-Gated Composite Random Activation (MCRA)*, resulting in the following update:

$$\mathbf{x}_t = \sigma_2(\mathbf{W}_1\mathbf{x}_{t-1} + \mathbf{W}_2\sigma_1(\mathbf{W}_{\text{in}}\mathbf{h}_t + \boldsymbol{\theta} + \mathbf{W}_0\mathbf{x}_{t-1})),$$

where \mathbf{W}_1 and \mathbf{W}_2 are matrix-valued gates constrained by normalization, and σ_1, σ_2 are nonlinear activation functions randomly selected from a predefined set (e.g., \tanh , ReLU , sigmoid).

The **MCRA** mechanism introduces four key novel elements:

- **Nonlinear Activation**: emphasizes that nonlinear transformations are applied both before and after the reservoir update, increasing expressiveness;
- **Matrix-Gated**: leaky integration is generalized using matrix-valued gates (replacing scalar α), allowing for more flexible and expressive dynamics;
- **Composite**: the activation is formed as a nested composition of two nonlinearities, enabling deeper feature transformations;
- **Randomized**: the nonlinear functions σ_1 and σ_2 are chosen randomly, encouraging diversity across the network ensemble.

This formulation allows for neuron-specific, nontrivial temporal dynamics and significantly enhances the representational capacity of the reservoir. The classical ESNs are recovered as a special case when σ_2 is the identity function and $\mathbf{W}_1, \mathbf{W}_2$ reduce to scalar weights.

2. **Heterogeneous Group X-ESNs for Stability**: To address the sensitivity of ESNs to random initialization, we propose **Group X-ESNs**: ensembles of independently initialized X-ESN units whose outputs are aggregated to produce a stable, low-variance memory stream. Specifically, we employ a heterogeneous group of X-ESNs, each with randomly assigned pair of activation functions and varying dimensions, to promote diversity. This approach reduces performance variance and improves robustness without compromising efficiency.
3. **Recurrent Dual-Stream for Token Selection**: We design a dual-stream architecture that combines Group X-ESNs (for long-range, non-i.i.d. dependencies) with a short-context base TSF model (e.g., PatchTST) trained on local, i.i.d. patterns. A cross-attention readout enables token-wise alignment, allowing the model to selectively attend to relevant historical states. This fusion effectively captures both persistent trends and local variations. Since the base model operates on a fixed-length window and X-ESNs are untrained reservoirs (no backpropagation), the overall training complexity remains linear in sequence length and constant per time step, with only the MLP readout layer and the cross-attention combiner trained via backpropagation.
4. **Standalone or Model Booster**: EFNS is a modular framework designed to perform time-series forecasting (TSF) either as a standalone model or as an enhancement for any baseline model, regardless of its architecture. We instantiate and evaluate multiple variants: **EchoSolo** (a standalone X-ESNs without any base model), **EchoFormer** (X-ESNs combined with PatchTST), **EchoMLP** (X-ESNs paired with an MLP), **X-ESNs** (X-ESNs integrated with TPGN), and **EchoLinear** (X-ESNs alongside DLinear). This flexibility enables the framework to adapt across diverse modeling paradigms and datasets, consistently delivering improved performance.

Results. EFNS achieves state-of-the-art performance across a range of multivariate TSF benchmarks. For example, on the DMV dataset, **EchoFormer** attains up to a **57.1% relative error reduction** compared to PatchTST, a leading Transformer-based model, as well as other state-of-the-art methods. This demonstrates EFNS' ability to capture deep temporal dependencies while maintaining linear computational complexity, with performance gains that increase as the forecasting horizon extends by leveraging the entire observed history.

2 ECHO FLOW NETWORKS

We enhance ESNs with scalar-value embedding, group **X-ESNs**, and a MLP readout with cross-attention combination. Each component is detailed below, followed by the complete algorithm.

2.1 BACKGROUND: TSF TASK AND BASE MODEL

In a rolling forecasting scenario with fixed context window k , the TSF goal is to predict future values $\hat{\mathbf{u}}_{t+1:t+\tau}$ from a short input sequence $\mathbf{u}_{t-k+1:t}$, here a time series dataset is denoted by $\mathbf{u}_{1:T}$ with $\mathbf{u}_t \in \mathbb{R}^{N_u}$. TSF task is expressed as:

$$\hat{\mathbf{u}}_{t+1:t+\tau} = \mathbb{M}(\mathbf{u}_{t-k+1:t}) \quad (2)$$

Here, $\mathbb{M}(\cdot)$ is a TSF **base model**, such as PatchTST, which serves both as a baseline to generate $\hat{\mathbf{u}}_{t+1:t+\tau}$ for comparison and as a component to generate $\hat{\mathbf{u}}'_{t+1:t+\tau}$ in Equation 9 for improvement.

2.2 SCALAR-VALUE EMBEDDING

Embedding Encoder (EE) To enhance semantic representation in time series forecasting, we adopt SCaNE (Huang et al., 2024) to map each scalar input $u_t \in \mathbb{R}^{N_u}$ into a dense vector, similar to word embeddings. This allows semantically similar values (e.g., 0°F and 100°F in traffic prediction) to be closer in the embedding space. The embedding process is defined as:

$$\mathbf{h}_t = \epsilon(\mathbf{u}_t), \quad \mathbf{h}_t \in \mathcal{R}^{E \times N_u}, \quad (3)$$

where $\epsilon(\cdot)$ is the **scalar-value embedding** function, and E is the embedding dimension.

Embedding Restoration Decoder (ERD) After prediction, a restoration decoder maps the high-dimensional embedding outputs $\hat{\mathbf{u}}'_{t+1:t+\tau} \in \mathbb{R}^{EN_u}$ back to the original scalar space $\hat{\mathbf{u}}_{t+1:t+\tau} \in \mathbb{R}^{N_u}$ using a single-layer feedforward network (FFN) with RLEU activation:

$$\hat{\mathbf{u}}_{t+1:t+\tau} = \tilde{\epsilon}(\hat{\mathbf{u}}'_{t+1:t+\tau}) = \text{FFN}(\hat{\mathbf{u}}'_{t+1:t+\tau}) \quad (4)$$

Here, FFN denotes the one-layer feedforward decoder used for dimensionality reduction, and $\hat{\mathbf{u}}'_{t+1:t+\tau}$ is the predictor output before restoring the embedding.

2.3 MATRIX-GATED COMPOSITE RANDOM ACTIVATION IN EXTENDED ESNs

To address the limited expressiveness and instability of classical ESNs, as defined in Equation 1, we introduce **Extended Echo State Networks (X-ESNs)**, which incorporate a novel mechanism called **Matrix-Gated Composite Random Activation (MCRA)**, which consists of three key elements: matrix-valued leaky parameters, cascaded composite activations, and randomized heterogeneous activation functions.

Matrix-Gated Leaky Integration Classical ESNs use a scalar leaky parameter α to interpolate between the current input and previous states. We generalize this by replacing α with diagonal matrices \mathbf{W}_1 and \mathbf{W}_2 , which gate the contribution of the previous state and current input, respectively. Unlike scalar mixing that only stretches and shrinks in the span, matrix-based gating supports a broader class of linear transformations, including scaling, rotation, shearing, and reflection, allowing state updates to move beyond the original span of input vectors, increasing learning capability.

Cascaded Composite Activations Specifically, we apply a pair of nonlinear functions (σ_1, σ_2) in a nested manner to replace the single \tanh in ESNs. This cascaded design increases representational capacity by stacking transformations: similar to how simple LEGO blocks can be stacked to form complex structures, this design enables neurons to approximate more complex, hierarchical dynamics. The result is a richer, neuron-specific control over memory decay and update strength.

Randomized and Heterogeneous Nonlinearities To further increase diversity and reduce overfitting, we introduce randomness into the choice of activation functions. Instead of a uniform \tanh across all neurons in ESNs, we randomly assign each **X-ESNs** unit a pair of nonlinearities (σ_1, σ_2)

drawn from a predefined set (e.g., `tanh`, `sigmoid`, `ReLU`, `leaky ReLU`). This ensemble of heterogeneous reservoirs, each with a unique activation signature, allows the model to capture a broader range of temporal dynamics and mitigates the risk of neuron inactivation or gradient vanishing. To bound activations for numerical stability, we apply normalization (i.e., `LayerNorm`) and clipping.

MCRA State Update Formally, the state update in **X-ESNs** of Equation 2 is refined as:

$$\mathbf{x}_t = \sigma_2(\mathbf{W}_1 \mathbf{x}_{t-1} + \mathbf{W}_2 \cdot \text{Clip}(\sigma_1(\text{Norm}(\mathbf{W}_{\text{in}} \mathbf{h}_t + \boldsymbol{\theta} + \mathbf{W} \mathbf{x}_{t-1})), -1, 1)), \quad (5)$$

where $\mathbf{x}_t \in \mathbb{R}^{N_r}$ is the reservoir state, $\mathbf{h}_t \in \mathbb{R}^{N_u}$ is the input embedding, and $\mathbf{W}_{\text{in}}, \mathbf{W}, \boldsymbol{\theta}$ are input, recurrent, and bias weights. \mathbf{W}_1 and \mathbf{W}_2 are matrix-valued leaky gates. The inner and outer activations (σ_1, σ_2) are randomly selected from a set of nonlinearities. The classical ESN is recovered when $\mathbf{W}_1, \mathbf{W}_2$ are scalars and $(\sigma_1, \sigma_2) = (\tanh, \text{linear})$.

2.4 MLP READOUT

To enhance expressiveness, we apply an MLP readout to each **X-ESNs**, transforming its internal states into fixed-dimensional, standardized representations. This nonlinear mapping captures rich dynamics while unifying diverse **X-ESNs** outputs to a fixed dimension for grouping:

$$\mathbf{y}_t = \phi_{\text{MLP}}(\mathbf{x}_t) = \sigma(\mathbf{W}_1 \mathbf{x}_t + \boldsymbol{\theta}_1), \quad \mathbf{y}_t \in \mathbb{R}^m \quad (6)$$

Here, ϕ_{MLP} is a learnable nonlinear function implemented as a feedforward neural network, which consists of one fully connected layer with a nonlinear activation function of `ReLU` $\sigma(\cdot)$. $\mathbf{W}_1 \in \mathbb{R}^{m \times N_r}$ is a learnable weight matrix that maps the **EFNs** with different output dimensions N_r into one unified dimension m , and $\boldsymbol{\theta}_1 \in \mathbb{R}^h$ is the bias vector.

2.5 GROUP X-ESNs

For stability, to mitigate sensitivity to random initialization of **X-ESNs** state weights, we introduce **Group X-ESNs**, an ensemble approach that reduces prediction variance for more stable outputs. Specifically, we integrate the MLP readouts of multiple independently initialized **Group X-ESNs** to improve stability. We consider L **X-ESNs**, each with distinct decay parameters and output dimension (ρ and N_r) as in Gallicchio et al. (2017), leading to a grouped representation \mathbf{o}_t formed by concatenating (\oplus) the outputs of all **X-ESNs** readouts:

$$\mathbf{o}_t = \mathbf{y}_t^1 \oplus \mathbf{y}_t^2 \oplus \dots \oplus \mathbf{y}_t^L \quad (7)$$

2.5.1 CROSS ATTENTION COMBINATION

We integrate long-term context from the group **X-ESNs** outputs \mathbf{o}_t (Equation 7) with short-term context from the k -window input embeddings $\mathbf{h}_{t-k+1:t}$. This fusion uses a cross-attention operator \uplus that both reads the group **X-ESNs** states relative to the task and merges them with recent short-term inputs. Multiple cross-attention layers are applied sequentially to combine $\mathbf{h}_{t-k+1:t}$ and \mathbf{o}_t :

$$\mathbf{h}_{t-k+1:t} \uplus \mathbf{o}_t = \text{LN} \left(\mathbf{o}_t + \text{DO} \left(\text{Softmax} \left(\frac{(\mathbf{o}_t \mathbf{W}^Q)(\mathbf{h}_{t-k+1:t} \mathbf{W}^K)^\top}{\sqrt{d_k}} \right) (\mathbf{h}_{t-k+1:t} \mathbf{W}^V) \right) \right) \quad (8)$$

Here, $\text{LN}(\cdot)$ denotes layer normalization (Ba et al., 2016), which standardizes activations across the hidden dimension, and $\text{DO}(\cdot)$ applies the dropout, a stochastic regularization mask to the attention output (Srivastava et al., 2014). $(\mathbf{W}^Q, \mathbf{W}^K, \mathbf{W}^V)$ are weights of query, key, and value, and d_k denotes the dimensionality of the keys. The fused representation, combining k -length context $\mathbf{h}_{t-k+1:t}$ with the **X-ESNs** states \mathbf{o}_t , is then passed into a base forecasting model \mathbb{M}_f , such as a Transformer-based model. The effective input length remains fixed at k , consistent with the baseline input size in Equation 2, and is significantly smaller than the full sequence length ($k \ll T$), ensuring computational efficiency as

$$\hat{\mathbf{u}}'_{t+1:t+\tau} = \tilde{\epsilon} \left(\mathbb{M}_f(\mathbf{h}_{t-k+1:t} \uplus \mathbf{o}_t) \right). \quad (9)$$

After predictions by \mathbb{M}_f , dimensions are restored via $\tilde{\epsilon}$ to yield the final outputs (see Equation 1).

2.6 TRAINING ALGORITHM

Algorithm 1 outlines the **EFNS** training procedure. The process begins with parameter initialization. Input sequences are embedded token-wise at each time step (**Step 1**). During each training step, every **X-ESNs** updates its internal states over the full context of length T , on non-i.i.d. data without backpropagation (**Step 2**). A fixed MLP readout is then applied to each **X-ESNs**'s state (**Step 3**), and the outputs of all L **X-ESNs** are concatenated to form the Group **X-ESNs** (**Step 4**), which is then fused with the embeddings of the short context with window size k via cross attention (**Step 5**), and are fed into a base model if available (**Step 6**). After that, the embeddings are restored (**Step 7**). The model is trained end-to-end via backpropagation (**Step 8**), by minimizing the standard Huber loss (Meyer, 2021) with details in Appendix A.

Algorithm 1 Training Algorithm

Require: $\mathbf{u}_{1:T}, \mathbb{M}_f(\cdot), \epsilon(\cdot), \hat{\epsilon}(\cdot)$
Ensure: Initialized $\mathbb{M}_f(\cdot)$

```

while  $epoch < epochs$  do
    for  $t \in T$  do
        ① Embedding Encoder [Eq. 3]
        for  $l \in L$  do
            ② EFNS [Eq. 5]
            ③ MLP Readout [Eq. 6]
        end for
        ④ Group EFNS [Eq. 7]
        ⑤ Joint Attention [Eq. 8]
        ⑥ Base Model [Eq. 9]
        ⑦ Embedding Restoration [Eq. 4]
        ⑧ Huber Loss Backpropagation
    end for
end while

```

3 EXPERIMENTS

We test five **EFNS** instantiations without and with different base models: **EchoSolo**: No base model is used; **EchoFormer**: Transformer-based model (PatchTST); **EchoMLP**: an MLP-based model (PatchTSTMixer); **EchoTPGN**: the 2D TSF model (TPGN); and **EchoLinear**: a decomposition-linear model (DLinear) base model, which combined the group **X-ESNs** at the back (see AppendixB).

3.1 EXPERIMENTAL SETTINGS

Evaluation Metrics and Datasets: We evaluate performance using Mean Squared Error (MSE) and Mean Absolute Error (MAE) (Hastie et al., 2009), where lower values are better. Benchmarks include representative TSF datasets: four ETT variants (ETTh1, ETTh2, ETTm1, ETTm2) (Zhou et al., 2021), Weather and Traffic (Zeng et al., 2022b), Air Quality (AQ) (De Vito et al., 2008), and Daily Website Visitors (DWV) (Hyndman, R. J.). For ETT, Weather, and Traffic, preprocessing follows (Zeng et al., 2022b), while AQ and DWV use a 70/10/20 split for training, validation, and testing.

Baselines: We compare **EFNS** against a range of strong baselines commonly used in TSF, including Transformer-based models such as PatchTST (Nie et al., 2023), Seg-RNN (Lin et al., 2023), MLP-based models like PatchTSTMixer (Ekambaram et al., 2023), linear projection models such as DLinear (Zeng et al., 2022b), and large pre-trained models like TimeLLM (Jin et al., 2024). The experimental setup follows the standardized protocol in (Zeng et al., 2022b) for fair comparison.

Model Parameters: We adopt the hyperparameter settings from Nie et al. (2023); Ekambaram et al. (2023); Toner & Darlow (2024). For PatchTST and PatchTSTMixer used as both baselines and base models in **EFNS**, we set FFN dimension to 256, dropout to 0.2, LayerNorm for FFN normalization, a fixed look-back window $k = 336$, patch length 16, stride 8, and 8 layers. For DLinear, we follow its original configuration Toner & Darlow (2024). All models use a learning rate of 1×10^{-3} as in Nie et al. (2023). Experiments are conducted on Tesla H100 GPUs using PyTorch Paszke et al. (2019) and HuggingFace Wolf et al. (2020). For large datasets like Weather, embeddings are optionally disabled to reduce memory usage. Full **EFNS** settings are in Appendix K, and variant details in Appendix C.

3.2 EVALUATION RESULTS

Results: Table 1 shows the TSF prediction results. Statistical significance is computed by running the same algorithm 10 times and averaging the results. Each of our **EFNS** realizations almost always outperforms its corresponding baselines, on three prediction horizons $h \in \{192, 336, 720\}$. **EchoLinear** outperforms DLinear, **EchoMLP** is better than PatchTSTMixer, and **EchoFormer** significantly improves over PatchTST and other baselines. Table 2 shows that **EchoFormer** significantly outper-

Table 1: EFNs family models compared with baselines including relative improvements (Rel. Imp. %).

Model	ETTh1 Dataset						DMV Dataset					
	192		336		720		192		336		720	
	MSE	MAE	MSE	MAE	MSE	MAE	MSE	MAE	MSE	MAE	MSE	MAE
DLinear	0.405	0.416	0.439	0.443	0.472	0.437	0.154	0.147	0.168	0.208	0.412	0.406
PatchTSMixer	0.400	0.433	0.426	0.457	0.433	0.469	0.138	0.123	0.183	0.226	0.395	0.381
PatchTST	0.379	0.256	0.435	0.462	0.447	0.472	0.142	0.106	0.172	0.212	0.427	0.404
EchoFormer	0.331	0.357	0.346	0.362	0.368	0.381	0.058	0.071	0.121	0.205	0.337	0.339
EchoSolo	0.391	0.399	0.420	0.459	0.441	0.466	0.117	0.104	0.166	0.231	0.393	0.385
EchoLinear	0.407	0.409	0.426	0.430	0.436	0.428	0.087	0.117	0.142	0.222	0.388	0.412
EchoMLP	0.382	0.403	0.408	0.419	0.417	0.452	0.093	0.114	0.162	0.253	0.379	0.362
Rel. Imp. %	-19.3	-15.89	-19.8	-17.3	-15.0	-13.56	-57.1	-31.5	-20.1	-1.5	-14.6	-12.9

Table 2: **EchoFormer** outperforms TSF baselines (horizons: {96, 192, 336, 720}).

Methods	Metric	EchoFormer (Ours)		DLinear		PatchTST		PatchTsMixer		Seg-RNN		TimeLMM		Rel. Imp. %	
		MSE	MAE	MSE	MAE	MSE	MAE	MSE	MAE	MSE	MAE	MSE	MAE	MSE	MAE
ETTh1	96	0.331 _{±0.0225}	0.346 _{±0.0163}	0.376	0.397	0.375	0.399	0.388	0.425	0.377	0.401	0.362	0.392	-9.2	-12.8
	192	0.338 _{±0.0143}	0.357 _{±0.0223}	0.405	0.416	0.413	0.421	0.400	0.433	0.422	0.441	0.416	0.425	-16.5	-14.2
	336	0.346 _{±0.0219}	0.362 _{±0.0152}	0.439	0.443	0.435	0.462	0.426	0.457	0.439	0.457	0.440	0.462	-18.8	-21.7
	720	0.368 _{±0.0227}	0.381 _{±0.0121}	0.472	0.490	0.447	0.472	0.433	0.469	0.434	0.447	0.450	0.462	-15.1	-19.8
ETTh2	avg	0.345	0.361	0.422	0.437	0.413	0.430	0.414	0.446	0.418	0.436	0.420	0.432	-17.3	-16.6
	96	0.273 _{±0.0148}	0.291 _{±0.0137}	0.289	0.353	0.274	0.336	0.334	0.355	0.263	0.322	0.277	0.350	3.5	-9.7
	192	0.293 _{±0.0144}	0.317 _{±0.0235}	0.383	0.418	0.339	0.379	0.341	0.380	0.337	0.372	0.355	0.380	-14.1	-16.4
	336	0.301 _{±0.0222}	0.321 _{±0.0236}	0.448	0.465	0.329	0.380	0.368	0.393	0.355	0.382	0.368	0.409	-8.6	-15.5
ETTm1	720	0.327 _{±0.0121}	0.355 _{±0.0126}	0.605	0.551	0.379	0.422	0.384	0.416	0.394	0.424	0.500	0.497	-14.8	-14.7
	avg	0.298	0.363	0.431	0.446	0.298	0.322	0.414	0.427	0.337	0.375	0.385	0.398	0	-3.2
	96	0.283 _{±0.0214}	0.322 _{±0.0218}	0.299	0.343	0.290	0.342	0.312	0.346	0.291	0.335	0.290	0.331	-2.8	-3.1
	192	0.331 _{±0.0121}	0.361 _{±0.0115}	0.335	0.365	0.332	0.369	0.348	0.374	0.366	0.381	0.347	0.369	-0.5	-1.1
ETTm2	336	0.358 _{±0.0142}	0.372 _{±0.0339}	0.369	0.386	0.366	0.392	0.410	0.411	0.388	0.401	0.357	0.385	0.4	-3.7
	720	0.401 _{±0.0241}	0.425 _{±0.0137}	0.425	0.421	0.416	0.420	0.405	0.418	0.412	0.418	0.409	0.436	-1.0	1.6
	avg	0.338	0.368	0.357	0.378	0.351	0.380	0.400	0.406	0.362	0.389	0.429	0.425	-3.8	-2.7
	96	0.180 _{±0.0213}	0.274 _{±0.0221}	0.187	0.269	0.165	0.255	0.167	0.267	0.158	0.241	0.170	0.277	13.9	12.4
Weather	192	0.196 _{±0.0126}	0.254 _{±0.0132}	0.224	0.303	0.220	0.292	0.233	0.275	0.215	0.283	0.236	0.273	-11.0	-6.7
	336	0.279 _{±0.0147}	0.341 _{±0.0139}	0.281	0.342	0.285	0.329	0.305	0.339	0.281	0.317	0.276	0.388	-2.2	7.5
	720	0.351 _{±0.0115}	0.383 _{±0.0191}	0.397	0.421	0.362	0.385	0.408	0.403	0.357	0.391	0.362	0.388	-2.7	-0.6
	avg	0.247	0.315	0.267	0.333	0.255	0.315	0.278	0.321	0.253	0.306	0.347	0.293	-2.4	2.9
Traffic	96	0.193 _{±0.0219}	0.205 _{±0.0227}	0.176	0.237	0.149	0.198	0.172	0.220	0.158	0.203	0.153	0.281	29.5	3.5
	192	0.201 _{±0.0224}	0.241 _{±0.0226}	0.220	0.282	0.213	0.244	0.217	0.247	0.201	0.247	0.196	0.257	-5.7	-1.3
	336	0.235 _{±0.0322}	0.257 _{±0.0319}	0.265	0.319	0.245	0.282	0.250	0.274	0.237	0.269	0.262	0.279	-0.9	-4.5
	720	0.302 _{±0.0233}	0.337 _{±0.0241}	0.333	0.362	0.325	0.357	0.319	0.339	0.311	0.348	0.304	0.356	-0.7	-3.2
Air Quality	avg	0.230	0.257	0.248	0.300	0.235	0.264	0.259	0.287	0.226	0.264	0.271	0.334	-2.2	-2.7
	96	0.288 _{±0.0328}	0.235 _{±0.0337}	0.410	0.282	0.360	0.249	0.367	0.357	0.543	0.255	0.388	0.264	-25.0	-6.6
	192	0.351 _{±0.0331}	0.256 _{±0.0328}	0.423	0.287	0.379	0.262	0.384	0.268	0.567	0.281	0.374	0.247	-7.4	-2.3
	336	0.362 _{±0.0328}	0.273 _{±0.0314}	0.436	0.296	0.392	0.269	0.393	0.268	0.602	0.307	0.385	0.271	-7.7	0.1
DMV	720	0.389 _{±0.0433}	0.281 _{±0.0423}	0.466	0.315	0.432	0.286	0.435	0.286	0.671	0.481	0.430	0.288	-10.0	-1.8
	avg	0.348	0.262	0.433	0.295	0.390	0.263	0.372	0.257	0.595	0.331	0.391	0.267	-11.5	-0.1
	96	0.494 _{±0.0299}	0.472 _{±0.0214}	0.569	0.601	0.541	0.538	0.511	0.535	0.526	0.566	0.519	0.526	-3.5	-11.3
	192	0.538 _{±0.0231}	0.519 _{±0.0178}	0.541	0.524	0.598	0.562	0.573	0.571	0.551	0.591	0.551	0.560	-0.4	-7.4
Weather	336	0.678 _{±0.0315}	0.632 _{±0.0322}	0.835	0.862	0.728	0.764	0.792	0.754	0.701	0.681	0.682	-0.5	-7.4	
	720	0.470	0.531	0.648	0.662	0.728	0.622	0.625	0.620	0.592	0.612	0.562	0.589	-16.4	-9.9
	avg	0.182	0.213	0.244	0.250	0.238	0.244	0.225	0.243	0.291	0.298	0.246	0.248	-28.7	-13.4

forms baseline models across most datasets in different horizons. Notably, **EchoFormer** achieves a deduction of MSE on the DMV dataset from 0.138 to 0.061, i.e., -57.1% relatively.

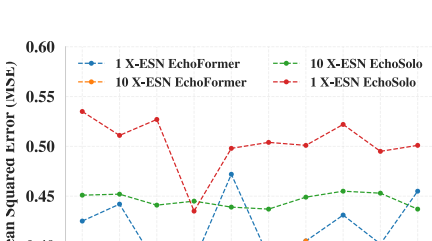


Figure 2: MSE vs. different initializations. Group EFNs (e.g., 10 EFNs) improve stability and error rates over a single EFNs on ETTh1. **EchoFormer** and **EchoSolo** are not sensitive to initialization.

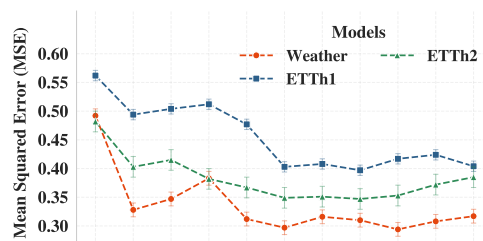


Figure 3: MSE vs. EFNs numbers. Optimal EFNs (e.g., 10 EFNs) improve stability and error rates over a single EFNs on ETTh1, ETTh2, and Weather.

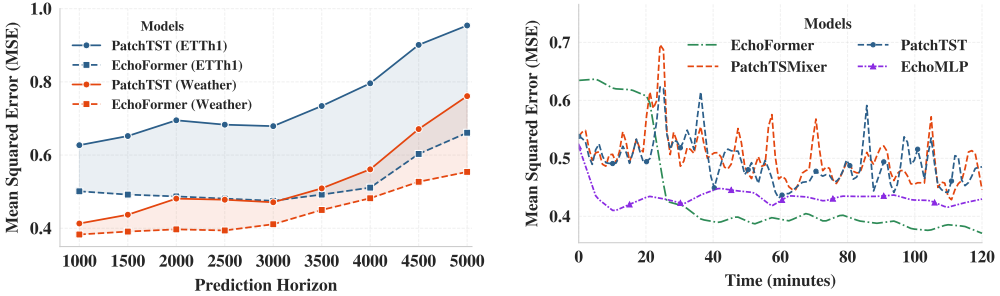


Figure 4: MSE vs. horizon length: **EchoFormer** outperforms the baseline across all horizons, with wider **EchoMLP** converge more quickly and achieve lower error rates than baselines on the ETTh1 validation set. (horizon 720 for all ablations by default).

Table 3: Training time (min) and memory (GB).

Dataset	EchoFormer min	EchoFormer GB	EchoSolo min	EchoSolo GB	PatchTST min	PatchTST GB	DLinear min	DLinear GB
ETTh1	32	12	10	3	40	10	14	4
ETTh2	33	12	9	4	40	10	16	4
ETTm1	57	18	17	6	60	16	25	7
ETTm2	57	19	20	6	60	16	24	8
Weather	47	155	15	30	48	130	21	34
Traffic	86	503	25	68	93	453	27	88

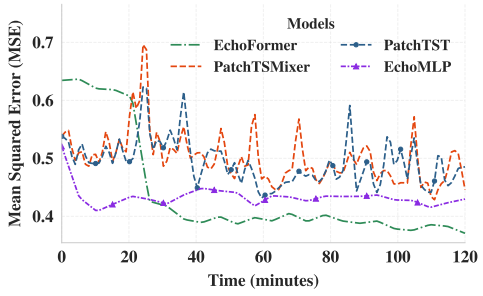


Figure 5: Model training efficiency. **EchoFormer** and **EchoMLP** converge more quickly and achieve lower error rates than baselines on the ETTh1 validation set.

Memory and Time Complexity Comparison: Let N_r be the **X-ESNs** state size, W the number of **X-ESNs**, k the short-term window, T the long-term input length, L the number of layers, r the compression ratio, P the patch size, and d_e the embedding dimension. The time and memory complexities of **X-ESNs** are $O(TN_r^2)$ and $O(N_r^2)$, respectively. For **EchoFormer**, the added cost from

PatchTST yields time complexity $O\left(\frac{T^2 d_e}{P^2} + N_r T k\right)$ and memory complexity $O\left(\frac{T^2 d_e}{P^2} + LT^2\right)$.

Despite its richer architecture, **EchoFormer** converges faster and achieves lower MSE than PatchTST, as shown in Figure 5. Training time, GPU usage, and efficiency metrics are summarized in Table 3.

3.3 ABLATION STUDY

Stability of Group X-ESNs: Figure 2 compares **EchoFormer** and **EchoSolo** under grouped (10 EFNS) and single (1 EFNS) configurations. Grouped **X-ESNs** exhibit significantly lower error and greater stability across runs, indicating reduced sensitivity to initialization.

Effect of Group Size: As shown in Figure 3, increasing the number of **X-ESNs** in the group leads to consistent improvements in MSE, with diminishing returns beyond size 10.

Forecast Horizon Robustness: Figure 4 shows our method outperforms baselines across all prediction horizons. The performance gap increases with longer horizons, demonstrating strong long-term forecasting capabilities.

Component Effectiveness: Table 4 reports ablation results on ETTh1, divided into three sections. The first shows baseline performance of PatchTST and TPGN. The second analyzes the impact of modifying or removing EchoFormer components. The third starts from classic ESNs Jaeger et al. (2007) and incrementally builds up with EFNS.

In the second section, removing scalar value embedding and its restoration causes a significant performance drop. Replacing cross-attention with concatenation or averaging also degrades results, confirming cross-attention’s superiority in fusing multi-source information. Increasing levels in the cascaded nonlinear activation function yields no further gain. Replacing randomized activations in **Group X-ESNs** with a single fixed function also reduces performance. Together, these results show each component contributes uniquely and synergistically to EchoFormer’s improvement.

Table 4: Component effectiveness on ETTh1.

Model	MSE	MAE
PatchTST	0.447	0.472
TPGN	0.519	0.541
EchoFormer	0.368	0.381
Without Embedding	0.465	0.490
Cross Attention → Concatenation	0.612	0.673
Cross Attention → Average	0.488	0.519
3 Level Composite	0.371	0.390
4 Level Composite	0.368	0.384
All MCRA Activation: ReLU	0.392	0.401
All MCRA Activation: Sigmoid	0.372	0.382
All MCRA Activation: tanh	0.375	0.390
1 ESN	0.681	0.657
2 1 + MLP Readout	0.627	0.606
3 2+ Group ESNs + Cross Attention	0.507	0.531
4 3+ tanh → Random	0.482	0.539
5 4+ MCRA (EchoSolo)	0.441	0.466
6 5+ TPGN (EchoTPGN)	0.462	0.481
7 5+ PatchTST (EchoFormer)	0.368	0.381

The third section uses system IDs in the first column to track incremental additions starting from classic ESNs (ID 1). The original ESN has high error, while adding an MLP readout (ID 2) reduces MSE. Further improvements come from Group ESNs and cross-attention, showcasing the power of the dual-stream and ensemble. Substituting \tanh with randomized activations further boosts performance. Integrating all **X-ESNs** components significantly lowers MSE (a 6.6% reduction). Combining **X-ESNs** with a moderate backbone like TPGN improves TPGN but is worse than EchoSolo, while a stronger backbone like PatchTST leads to the best overall performance in EchoFormer.

4 RELATED WORK

Deep Learning for TSF Recent TSF models span CNNs (e.g., MICN (Wang et al., 2023), TimesNet (Wu et al., 2023), ModernTCN (Luo & Wang, 2024)) for local patterns; RNNs (e.g., SegRNN (Lin et al., 2023), WITRAN (Jia et al., 2023)) for sequential modeling but prone to gradient issues; and linear models (e.g., FITS (Xu et al., 2024), SparseTSF (Lin et al., 2024b), CycleNet (Lin et al., 2024a)) which are efficient but less expressive. Transformers (e.g., PatchTST (Nie et al., 2023), TiDE (Huang, 2023), FiLM (Wang, 2023), BasisFormer (Zhou, 2023), iTransformer (Liu et al., 2024), Leddam (Yu et al., 2024)) achieve high accuracy but with high cost. PatchTST (Nie et al., 2023) and SegRNN (Lin et al., 2023) perform well but struggle with fine-grained or irregular inputs (Nie et al., 2023; Lin et al., 2023). TimeKAN (Huang et al., 2025) prioritizes efficiency, while TPGN (Jia et al., 2024) risks future leakage (Chi, 2024). **EFNS** mitigates these by learning full history without backpropagation through time, combining accuracy with scalability.

ESN Efficiency and Stability ESNs avoid vanishing gradients by using fixed recurrent weights (Jaeger, 2001), requiring no backpropagation through time. They offer constant memory and optimization costs ($\mathcal{O}(1)$) via lightweight readouts. Approaches such as spectral radius tuning (Lukoševičius & Jaeger, 2009), regularization (Rodan & Tiňo, 2011), and reservoir optimization (Lu et al., 2017) aim to stabilize ESNs but often need careful tuning. **EFNS** instead aggregates multiple randomly initialized Group X-ESNs and integrates them via cross-attention—more adaptive than prior parallel reservoirs (Sun et al., 2024; Casanova et al., 2023; Rodan & Tiňo, 2011). Furthermore, ESNs suffer from initialization sensitivity and limited readout expressiveness. Prior work explores spectral tuning (Jaeger, 2001; Rodan & Tiňo, 2011), nonlinear readouts (Gauthier et al., 2021b), attention (Ma et al., 2022), and graph-based methods (Liao, 2023). **EFNS** unifies ESNs with a dual-stream architecture and attention-based readout for improved accuracy and adaptability.

Expressive Readouts and Modular Architectures Classic ESNs use linear readouts (Jaeger et al., 2007; Jaeger, 2001), while recent works explore quadratic (Gauthier et al., 2021b), kernel (Hermans & Schrauwen, 2010), or attention-based mappings (Köster & Anandkumar, 2025), often trading efficiency for expressiveness. **EFNS** outperforms in both accuracy and efficiency. Additionally, although ESNs have been embedded into neural architectures (Sun et al., 2024; Xu et al., 2025; Casanova et al., 2023; Shen et al., 2020), they typically serve fixed roles; **EFNS**’ cross-attention readout enables flexible model compositions, yielding multiple effective variants.

5 CONCLUSION

ECHO FLOW NETWORKS is a powerful and flexible framework for capturing long-term temporal dependencies, consistently improving performance both standalone and as an enhancer to existing TSF models. This work is the first to demonstrate that ESNs can enhance Transformer-based TSF models, highlighting a promising direction for efficient, scalable sequence modeling. We hope this advances future research on ESN-based architectures in accuracy and scalability.

6 IMPACT STATEMENT

This work improves TSF with social values.

Reproducibility statement **EFNS**’ source code is in the supplementary materials. Experimental details and dataset info are in Section 5 and Appendix K.

REFERENCES

Ba JL, Kiros JR, Hinton GE. Layer normalization. arXiv preprint arXiv:1607.06450. 2016 Jul 21.

Bollt E. On explaining the surprising success of reservoir computing forecaster of chaos? The universal machine learning dynamical system with contrast to VAR and DMD. *Chaos: An Interdisciplinary Journal of Nonlinear Science*. 2021 Jan 1;31(1).

Wen Q, Zhou T, Zhang C, Chen W, Ma Z, Yan J, Sun L. Transformers in time series: A survey. arXiv preprint arXiv:2202.07125. 2022 Feb 15.

Casanova M, Dalena B, Bonaventura L, Giovannozzi M. Ensemble reservoir computing for dynamical systems: prediction of phase-space stable region for hadron storage rings. *The European Physical Journal Plus*. 2023 Jun 1;138(6):559.

Chen L, Chen D, Shang Z, Wu B, Zheng C, Wen B, Zhang W. Multi-scale adaptive graph neural network for multivariate time series forecasting. *IEEE Transactions on Knowledge and Data Engineering*. 2023 Apr 19;35(10):10748-61.

Jia Y, Lin Y, Yu J, Wang S, Liu T, Wan H. PGN: The RNN's New Successor is Effective for Long-Range Time Series Forecasting. *Advances in Neural Information Processing Systems*. 2024 Dec 16;37:84139-68.

Cho K, Van Merriënboer B, Gulcehre C, Bahdanau D, Bougares F, Schwenk H, Bengio Y. Learning phrase representations using RNN encoder-decoder for statistical machine translation. arXiv preprint arXiv:1406.1078. 2014 Jun 3.

De Vito S, Massera E, Piga M, Martinotto L, Di Francia G. On field calibration of an electronic nose for benzene estimation in an urban pollution monitoring scenario. *Sensors and Actuators B: Chemical*. 2008 Feb 22;129(2):750-7.

Ekambaram V, Jati A, Nguyen N, Sinthong P, Kalagnanam J. Tsmixer: Lightweight mlp-mixer model for multivariate time series forecasting. In *Proceedings of the 29th ACM SIGKDD conference on knowledge discovery and data mining* 2023 Aug 6 (pp. 459-469).

Gallicchio C, Micheli A, Pedrelli L. Deep reservoir computing: A critical experimental analysis. *Neurocomputing*. 2017 Dec 13;268:87-99.

Gauthier DJ, Bollt E, Griffith A, Barbosa WA. Next generation reservoir computing. *Nature communications*. 2021 Sep 21;12(1):5564.

Hastie T. The elements of statistical learning: data mining, inference, and prediction.

Grezen F. Reservoir Computing: A New Paradigm for Neural Networks. arXiv preprint arXiv:2504.02639. 2025 Apr 3.

Graves A. Long short-term memory. Supervised sequence labelling with recurrent neural networks. 2012 Feb 6:37-45.

Huang CK, Hsieh YH, Chien TJ, Chien LC, Sun SH, Su TH, Kao JH, Lin C. Scalable Numerical Embeddings for Multivariate Time Series: Enhancing Healthcare Data Representation Learning. arXiv preprint arXiv:2405.16557. 2024 May 26.

Das A, Kong W, Leach A, Mathur S, Sen R, Yu R. Long-term forecasting with tide: Time-series dense encoder. arXiv preprint arXiv:2304.08424. 2023 Apr 17.

Huang S, Zhao Z, Li C, Bai L. Timekan: Kan-based frequency decomposition learning architecture for long-term time series forecasting. arXiv preprint arXiv:2502.06910. 2025 Feb 10.

Jaeger H. Echo state network. *scholarpedia*. 2007 Sep 6;2(9):2330.

Jaeger H, Lukoševičius M, Popovici D, Siewert U. Optimization and applications of echo state networks with leaky-integrator neurons. *Neural networks*. 2007 Apr 1;20(3):335-52.

Jia Y, Lin Y, Hao X, Lin Y, Guo S, Wan H. Witran: Water-wave information transmission and recurrent acceleration network for long-range time series forecasting. *Advances in Neural Information Processing Systems*. 2023 Dec 15;36:12389-456.

Jia Y, Lin Y, Yu J, Wang S, Liu T, Wan H. PGN: The RNN's New Successor is Effective for Long-Range Time Series Forecasting. *Advances in Neural Information Processing Systems*. 2024 Dec 16;37:84139-68.

Jin M, Wang S, Ma L, Chu Z, Zhang JY, Shi X, Chen PY, Liang Y, Li YF, Pan S, Wen Q. Time-Ilm: Time series forecasting by reprogramming large language models. *arXiv preprint arXiv:2310.01728*. 2023 Oct 3.

Kitaev N, Kaiser Ł, Levskaya A. Reformer: The efficient transformer. *arXiv preprint arXiv:2001.04451*. 2020 Jan 13.

Köster F, Kanno K, Uchida A. Attention-Enhanced Reservoir Computing as a Multiple Dynamical System Approximator. *arXiv preprint arXiv:2505.05852*. 2025 May 9.

Singh P, Sharma M, Dey A, Raman B. Frozen in Time: Parameter-Efficient Time Series Transformers via Reservoir-Induced Feature Expansion and Fixed Random Dynamics. *arXiv preprint arXiv:2508.18130*. 2025 Aug 25.

Gan T, Xu B, Li J. Transportation Flow Prediction Based on Graph Attention Echo State Network. *InProceedings of the 2023 4th International Conference on Computing, Networks and Internet of Things 2023* May 26 (pp. 708-713).

Lim B, Zohren S. Time-series forecasting with deep learning: a survey. *Philosophical Transactions of the Royal Society A*. 2021 Apr 5;379(2194):20200209.

Lin S, Lin W, Wu W, Zhao F, Mo R, Zhang H. Segrrnn: Segment recurrent neural network for long-term time series forecasting. *arXiv preprint arXiv:2308.11200*. 2023 Aug 22.

Lin S, Lin W, Hu X, Wu W, Mo R, Zhong H. Cyclenet: Enhancing time series forecasting through modeling periodic patterns. *Advances in Neural Information Processing Systems*. 2024 Dec 16;37:106315-45.

Lin S, Lin W, Wu W, Chen H, Yang J. Sparsesf: Modeling long-term time series forecasting with 1k parameters. *arXiv preprint arXiv:2405.00946*. 2024 May 2.

Liu Y, Hu T, Zhang H, Wu H, Wang S, Ma L, Long M. itransformer: Inverted transformers are effective for time series forecasting. *arXiv preprint arXiv:2310.06625*. 2023 Oct 10.

Lu Z, Pathak J, Hunt B, Girvan M, Brockett R, Ott E. Reservoir observers: Model-free inference of unmeasured variables in chaotic systems. *Chaos: An Interdisciplinary Journal of Nonlinear Science*. 2017 Apr 1;27(4).

Lukoševičius M, Jaeger H. Reservoir computing approaches to recurrent neural network training. *Computer science review*. 2009 Aug 1;3(3):127-49.

Luo D, Wang X. Modernncn: A modern pure convolution structure for general time series analysis. *InThe twelfth international conference on learning representations 2024* May 7 (pp. 1-43).

Ma C, Hou Y, Li X, Sun Y, Yu H. Long Input Sequence Network for Long Time Series Forecasting. *arXiv preprint arXiv:2407.15869*. 2024 Jul 18.

Lyu H, Huang D, Li S, Ng WW, Ma Q. Multiscale echo self-attention memory network for multivariate time series classification. *Neurocomputing*. 2023 Feb 1;520:60-72.

Meyer GP. An alternative probabilistic interpretation of the huber loss. *InProceedings of the ieee/cvpr conference on computer vision and pattern recognition 2021* (pp. 5261-5269).

Nie Y. A Time Series is Worth 64Words: Long-term Forecasting with Transformers. *arXiv preprint arXiv:2211.14730*. 2022.

Paszke A, Gross S, Massa F, Lerer A, Bradbury J, Chanan G, Killeen T, Lin Z, Gimelshein N, Antiga L, Desmaison A. Pytorch: An imperative style, high-performance deep learning library. *Advances in neural information processing systems*. 2019;32.

Rodan A, Tino P. Minimum complexity echo state network. *IEEE transactions on neural networks*. 2010 Nov 11;22(1):131-44.

Shen S, Baevski A, Morcos A, Keutzer K, Auli M, Kiela D. Reservoir transformers. InProceedings of the 59th Annual Meeting of the Association for Computational Linguistics and the 11th International Joint Conference on Natural Language Processing (Volume 1: Long Papers) 2021 Aug (pp. 4294-4309).

Gong Z, Tang Y, Liang J. Patchmixer: A patch-mixing architecture for long-term time series forecasting. arXiv preprint arXiv:2310.00655. 2023 Oct 1.

Srivastava N, Hinton G, Krizhevsky A, Sutskever I, Salakhutdinov R. Dropout: a simple way to prevent neural networks from overfitting. *The journal of machine learning research*. 2014 Jan 1;15(1):1929-58.

Sun J, Li L, Peng H, Liu S. Multidimensional Nonlinearity Time Series Forecasting Based on Multi-reservoir Echo State Network. InInternational Conference on Nonlinear Dynamics and Applications 2023 Jun 18 (pp. 81-90). Cham: Springer Nature Switzerland.

Tiňo P, Hammer B, Bodén M. Markovian bias of neural-based architectures with feedback connections. InPerspectives of neural-symbolic integration 2007 (pp. 95-133). Berlin, Heidelberg: Springer Berlin Heidelberg.

Toner W, Darlow L. An analysis of linear time series forecasting models. arXiv preprint arXiv:2403.14587. 2024 Mar 21.

Vaswani A, Shazeer N, Parmar N, Uszkoreit J, Jones L, Gomez AN, Kaiser Ł, Polosukhin I. Attention is all you need. *Advances in neural information processing systems*. 2017;30.

Vlachas PR, Pathak J, Hunt BR, Sapsis TP, Girvan M, Ott E, Koumoutsakos P. Backpropagation algorithms and reservoir computing in recurrent neural networks for the forecasting of complex spatiotemporal dynamics. *Neural Networks*. 2020 Jun 1;126:191-217.

Hospedales T, Antoniou A, Micaelli P, Storkey A. Meta-learning in neural networks: A survey. *IEEE transactions on pattern analysis and machine intelligence*. 2021 May 11;44(9):5149-69.

Zhou T, Ma Z, Wen Q, Sun L, Yao T, Yin W, Jin R. Film: Frequency improved legendre memory model for long-term time series forecasting. *Advances in neural information processing systems*. 2022 Dec 6;35:12677-90.

Wang H, Peng J, Huang F, Wang J, Chen J, Xiao Y. Micn: Multi-scale local and global context modeling for long-term series forecasting. InThe eleventh international conference on learning representations 2023.

Wolf T, Debut L, Sanh V, Chaumond J, Delangue C, Moi A, Cistac P, Rault T, Louf R, Funtowicz M, Davison J. Transformers: State-of-the-art natural language processing. InProceedings of the 2020 conference on empirical methods in natural language processing: system demonstrations 2020 Oct (pp. 38-45).

Shao Z, Zhang Z, Wang F, Xu Y. Pre-training enhanced spatial-temporal graph neural network for multivariate time series forecasting. InProceedings of the 28th ACM SIGKDD conference on knowledge discovery and data mining 2022 Aug 14 (pp. 1567-1577).

Garza A, Challu C, Mergenthaler-Canseco M. TimeGPT-1. arXiv preprint arXiv:2310.03589. 2023 Oct 5.

Wu H, Hu T, Liu Y, Zhou H, Wang J, Long M. Timesnet: Temporal 2d-variation modeling for general time series analysis. arXiv preprint arXiv:2210.02186. 2022 Oct 5.

Wu H, Xu J, Wang J, Long M. Autoformer: Decomposition transformers with auto-correlation for long-term series forecasting. *Advances in neural information processing systems*. 2021 Dec 6;34:22419-30.

Xu Y, Gottwald GA, Kuncic Z. Dynamic Reservoir Computing with Physical Neuromorphic Networks. *arXiv preprint arXiv:2505.16813*. 2025 May 22.

Xu Z, Zeng A, Xu Q. FITS: Modeling time series with 10^k parameters. *arXiv preprint arXiv:2307.03756*. 2023 Jul 6.

Yu G, Zou J, Hu X, Aviles-Rivero AI, Qin J, Wang S. Revitalizing multivariate time series forecasting: Learnable decomposition with inter-series dependencies and intra-series variations modeling. *arXiv preprint arXiv:2402.12694*. 2024 Feb 20.

Zeng A, Chen M, Zhang L, Xu Q. Are transformers effective for time series forecasting?. In *Proceedings of the AAAI conference on artificial intelligence* 2023 Jun 26 (Vol. 37, No. 9, pp. 11121-11128).

Hyndman, R. J., Athanasopoulos, G. (n.d.). DWV dataset [Data set]. StatForecasting.com. Retrieved October 26, 2023, from <https://regressit.com/statforecasting.html>

Ni Z, Yu H, Liu S, Li J, Lin W. Basisformer: Attention-based time series forecasting with learnable and interpretable basis. *Advances in Neural Information Processing Systems*. 2023 Dec 15;36:71222-41.

Zhou H, Zhang S, Peng J, Zhang S, Li J, Xiong H, Zhang W. Informer: Beyond efficient transformer for long sequence time-series forecasting. In *Proceedings of the AAAI conference on artificial intelligence* 2021 May 18 (Vol. 35, No. 12, pp. 11106-11115).

Appendices

A TRAINING LOSS

Our loss function (Meyer, 2021) is as follows:

$$\mathcal{L}(\bar{\mathbf{u}}_{t+1:t+\tau}, \hat{\mathbf{u}}_{t+1:t+\tau}) = \frac{1}{\tau} \sum_{i=t+1}^{t+\tau} \ell(\bar{\mathbf{u}}_i, \hat{\mathbf{u}}_i) \quad (10)$$

$$\ell(\bar{\mathbf{u}}_i, \hat{\mathbf{u}}_i) = \begin{cases} \frac{1}{2}(\bar{\mathbf{u}}_i - \hat{\mathbf{u}}_i)^2, & \text{if } |\bar{\mathbf{u}}_i - \hat{\mathbf{u}}_i| \leq \delta \\ \delta (|\bar{\mathbf{u}}_i - \hat{\mathbf{u}}_i| - \frac{1}{2}\delta), & \text{otherwise} \end{cases}$$

Here, δ sets the differentiability threshold; $\bar{\mathbf{u}}_i$ is the label and $\hat{\mathbf{u}}_i$ the prediction at time i .

As an example, we illustrate how **X-ESNs** outputs are paired with embedded inputs when the look-back window is set to $k = 2$. At each step, the **X-ESNs** state is updated by incorporating the current input h_t into the previous state x_{t-1} , yielding the new state x_t . For instance, x_1 is initialized from h_1 , x_2 is obtained by reading h_2 into x_1 , and x_3 is obtained by reading h_3 into x_2 . With $k = 2$, future predictions $\hat{\mathbf{u}}_{4:4+\tau}$ are generated via cross-attention between step-3 states (x_3) and the inputs $h_{2:3}$.

For the next time step, we read the h_4 value into step 3's states and generate step 4's states. By using the cross attention between step 4's states after linear transformation and $h_{3:4}$, we can make our future prediction $\hat{\mathbf{u}}_{5:5+\tau}$.

B ECHO FLOW NETWORKS MODEL ARCHITECTURES WITH FRONT AND END COMBINER

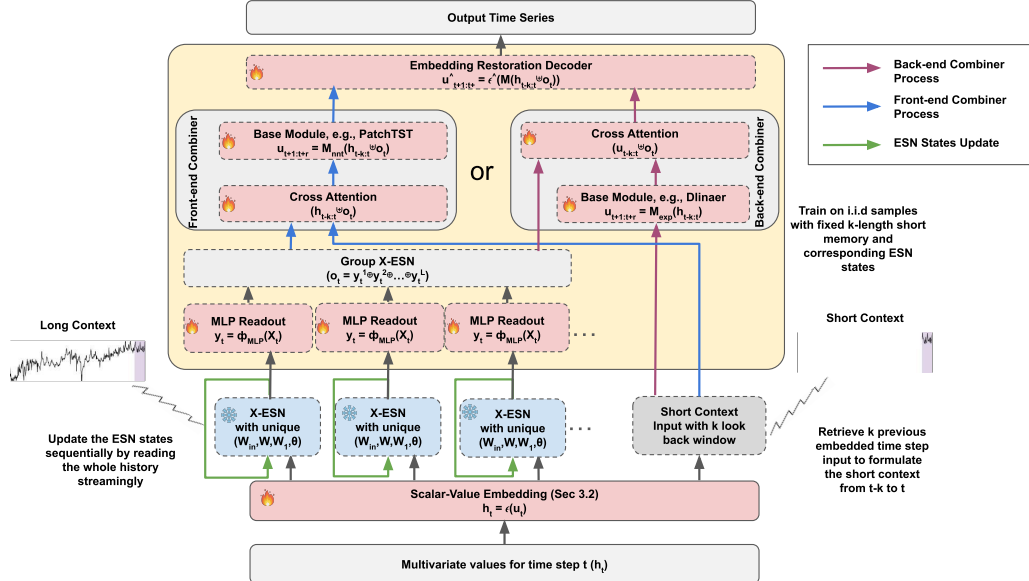


Figure 6: **ECHO FLOW NETWORKS** Models Structure. The components in red are trainable, and those in blue are frozen. Meanwhile, the Green arrows for Reservoirs represent the reservoir state updating process, current reservoir state will be one input for the Reservoir in the next time step. The blue and pink arrow represent the Front-end (Front) and Back-end Combiner.

C ECHO FLOW NETWORKS FAMILY DESCRIPTION

- **EchoSolo:** EchoSolo use the standalone group **X-ESNs** as a TSF predictor, consisting of the Scaler-Value Embedding, Group **X-ESNs** and Front-end (Front) Combiner. EchoSolo uses a Front-end (Front) Combiner, combining the **X-ESNs** output with the actual time series input. Then the outputs are fed into the Embedding Restoration Decoder to restore their shape back to the input shape before the Scaler-Value Embedding to generate the final prediction outputs.
- **EchoFormer:** EchoFormer combines Group **X-ESNs** and the Transformer-based PatchTST TSF model. Specifically, EchoFormer consists the Scalar-Value Embedding, Group **X-ESNs** and Front-end (Front) Combiner. Following Equation 8, then the results from the Front-end (Front) Combiner are fed into a PatchTST model following the setting pointed in the Model Parameters section. Then, the outputs of the PatchTST model are feed into the Embedding Restoration Decoder to shift the dimension of these outputs back into their original input dimension to generate the final prediction outputs.
- **EchoMLP:** EchoMLP combines Group **X-ESNs** and MLP-based PatchTSTMixer. Specifically, EchoMLP also include the Scalar-Value Embedding, Group **X-ESNs** and Front-end (Front) Combiner, then the results from the Front-end (Front) Combiner are fed into a PatchTSTMixer model following the settings in the Model Parameters section. In the end, the PatchTSTMixer model predictions are shifted by Embedding Restoration Decoder to the original input shapes and generate the final outputs.
- **EchoLinear:** EchoLinear combines Group **X-ESNs** with decomposition and linear modeling method of DLinear. Unlike previous models, EchoLinear model applied the Back-end (Back) Combiner, the time series inputs first go through the Scaler-Value Embedding layer to expand the dimension of the inputs, then the embedded inputs are fed into the Dlinear model to generate the time series predictions. These predictions from Dlinear model are then corrected and improved by the **X-ESNs** outputs through the Back-end (Back) Combiner explained in Equation 8. The Back-end (Back) Combiner here effectively injects long-range dependencies into Dlinear model’s outputs. Finally, the Embedding Restoration Decoder reconstructs the combined high-dimensional results back to the original prediction space and generate the final predictions.
- **EchoTPGN:** EchoTPGN integrates an Extented Echo State Network (**EFNS**) with a convolutional network-based TPGN model. Similar to EchoLinear, we employ the Back-end (Back) Combiner for TPGN. However, to maintain the effectiveness of the convolutional layers within TPGN, the model inputs are fed directly to TPGN without scaler values embedding. The future predictions generated by TPGN are then combined with the group **X-ESNs** results via cross-attention layers, stabilizing the overall predictions. Crucially, EchoTPGN preserves the original input shape and structure required by the TPGN model, maximizing the utility of its internal convolutional layers.

D FRONT AND BACK COMBINER

For cross-attention readout, we consider two distinct settings. For neural network-based base models, such as PatchTST, we employ a front combiner to leverage the features learned by the **X-ESNs** groups. In contrast, frequency analytical base models like DLinear, we use a back combiner that directly exploits the inherent structure of the input data to extract features, as follows:

$$\hat{\mathbf{u}}'_{t+1:t+\tau} = \begin{cases} \tilde{\epsilon} \left(\mathbb{M}_f(\mathbf{h}_{t-k+1:t} \uplus \mathbf{o}_t) \right) & \text{Front} \\ \tilde{\epsilon} \left(\mathbb{M}_b(\mathbf{h}_{t-k+1:t}) \uplus \mathbf{o}_t \right) & \text{Back} \end{cases} \quad (11)$$

Front We use cross attention to combine \uplus the embedded input $\mathbf{h}_{t-k+1:t}$ and the group **X-ESNs** output \mathbf{o}_t and then feed into the base model like PatchTST and generate the prediction $\hat{\mathbf{u}}'_{t+1:t+\tau}$ through:

$$\hat{\mathbf{u}}'_{t+1:t+\tau} = \tilde{\epsilon} \left(\mathbb{M}_f(\mathbf{h}_{t-k+1:t} \uplus \mathbf{o}_t) \right) \quad (12)$$

The resulting effective input size to the base model is the same as the baseline input size as in the baseline model, which is significantly smaller than the all-time history length, $k \ll T$.

Back Unlike the front combiner, the back combiner integrates the output from the base model like Dlinear, with the Group **X-ESNs** states \mathbf{o}_t following:

$$\hat{\mathbf{u}}'_{t+1:t+\tau} = \tilde{\epsilon} \left(\mathbb{M}_b(\mathbf{h}_{t-k+1:t}) \uplus \mathbf{o}_t \right) \quad (13)$$

The back combiner is designed especially for decomposition-based models like Dlinear etc....

Table 5: Additional Component Ablation Study

Models	MSE	MAE
EchoFormer	0.368	0.381
MSE as loss function	0.362	0.395
with Leaky value α	0.372	0.387

E LEAKY WEIGHTS AND VALUES COMPARISON

Table 5 also shows that changing the leaky value mechanism to the leaky weights mechanism yields significant improvements in our model, from about 0.372 to about 0.368.

F LOSS FUNCTION COMPARISON

Table 5 shows that although using MSE as a loss function can reach a slightly lower MSE level, the MAE performance is not ideal compared to using Huber loss as a loss function, which effectively ensures the convergence of both MAE and MSE during training.

G EXTENDED ECHO STATE NETWORK SIZE ANALYSIS

Our optimized **X-ESNs** state size is (100, 105, 110, 115, 120, 125, 130, 135, 140, 145, 150) and the number of **X-ESNs** is 10 as in Figure 7 and Figure 3 for all **ECHO FLOW NETWORKS** family models. The optimized spectral radius values are (0.9, 0.85, 0.80, 0.75, 0.7, 0.65, 0.6, 0.55, 0.5, 0.45) for each **X-ESNs** in the group.

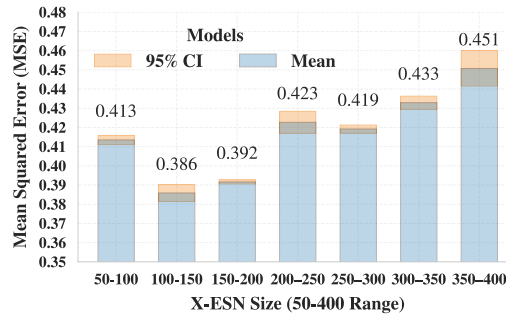


Figure 7: MSE vs. **X-ESNs** size.

Figure 7 shows that **X-ESNs** size significantly affects performance. Testing sizes from 50 to 100 reveals an optimal range of 100–150, roughly $0.8 \sim 1.0 \times E$. Smaller **X-ESNs** lack capacity; larger ones overfit. Proportional sizing to the embedding dimension is key for stable learning.

Table 6: Detailed hyperparameter settings for the group **X-ESNs**

X-ESNs ID	X-ESNs Size	Spectral Radius	Sparsity	MCRA
X-ESNs-1	100	0.90	0.60	Tanh
X-ESNs-2	105	0.85	0.55	Sigmoid
X-ESNs-3	110	0.80	0.50	Relu
X-ESNs-4	115	0.75	0.45	Tanh
X-ESNs-5	120	0.70	0.40	Sigmoid
X-ESNs-6	125	0.65	0.35	Relu
X-ESNs-7	130	0.60	0.30	Tanh
X-ESNs-8	135	0.55	0.25	Sigmoid
X-ESNs-9	140	0.50	0.20	Relu
X-ESNs-10	145	0.45	0.15	Tanh

H COMPLEXITY RANKING OF TIME SERIES FORECASTING METHODS

Table 7: Complexity of time series forecasting methods with theoretical training, practical training (frozen parts), inference, and memory costs. RNN (LSTM/GRU) Hochreiter & Schmidhuber (1997); Cho et al. (2014) Transfer Learning (Frozen Base) Borovykh et al. (2022). Meta-Learning (HyperNet) von Oswald et al. (2019). Foundation Model + Adapter (TimeGPT) Wu (2023b). Frozen Transformer Encoder Li & Wang (2022)

Rank	Method	Trainable Part	Training Time Complexity (full model)	Practical Training Time (frozen parts)	Inference Time
1	ESN Jaeger (2001)	Output layer only	$\mathcal{O}(N^2T + N^3)$	Same as full	$\mathcal{O}(NT)$
2	DLinear Zeng et al. (2022b)	Entire model	$\mathcal{O}(DTB)$	Same as full	$\mathcal{O}(DT)$
3	RNN (LSTM/GRU)	Entire model	$\mathcal{O}(DTB)$	Same as full	$\mathcal{O}(DT)$
4	Transfer Learning (Frozen Base)	Head only	$\mathcal{O}(DTB)$	$\mathcal{O}(D_{head}TB)$	$\mathcal{O}(L^2H)$
5	PatchTSMixer Song et al. (2023)	Entire mixer	$\mathcal{O}(DTB)$	Same as full	$\mathcal{O}(DT)$
6	PatchTST Nie et al. (2023)	Entire transformer	$\mathcal{O}(L^2HB)$	Same as full	$\mathcal{O}(L^2H)$
7	Frozen Transformer Encoder	Head only	$\mathcal{O}(D_{head}TB)$	≈ 0 (frozen encoder)	$\mathcal{O}(L^2H)$
8	Meta-Learning (HyperNet)	Meta-network	$\mathcal{O}(D_{meta}TB)$	Same as full	$\mathcal{O}(D_{generated}T)$
9	TPGN Wu (2023a)	Entire GNN + temporal layers	High (graph conv + temporal layers)	Same as full	Moderate-High
10	TimeGPT	Adapter/head only	$\mathcal{O}(D_{adapter}TB)$	≈ 0 (frozen backbone)	$\mathcal{O}(L^2H)$
Memory Complexity			\approx weights + activations + inputs; typically $\mathcal{O}(\text{model size} + L \cdot d_{model})$ for deep models		

We show complexity in theory in Table 7 with following notations:

- **Theoretical training time complexity:** Cost when training *all* trainable parameters.
- **Practical training time:** Cost when *no* network part is trained or only small heads/adapters are trained (frozen backbone).
- **Inference time complexity:** Cost for forward pass to produce predictions.
- **Memory complexity:** RAM/GPU memory use to store weights, activations, and inputs.

The variable definitions are as follows:

- T : length of the time series (sequence length)
- B : batch size during training
- L : input context length or window size (for transformers and patch models)
- H : number of layers in deep models (e.g., transformer layers)
- N : number of neurons in the reservoir (for ESN)
- D : number of trainable parameters in a model or specific module (head, adapter, etc.)
- M : number of tasks or meta-learning episodes
- d_{model} : model hidden dimension size (transformer embedding dimension)

Below are details of each method:

- **ESN** trains only the output layer, making both training and inference efficient.
- **DLinear** and **RNN** train the entire network, so practical training is equal to theoretical.

- **Transfer learning** freezes the backbone and trains a small head, reducing practical training time.
- **Frozen Transformer Encoder** and **Foundation Models** typically have near-zero training cost since the backbone is frozen and only adapters or heads are trained.
- **Meta-learning** requires expensive meta-training but fast adaptation at inference.
- **TPGN** fully trains GNN + temporal components, so practical training is as costly as theoretical.

I COMPLEXITY ANALYSIS

Model	Memory	Time
Transformer	$O(L^2 + Ld)$	$O(T^2 d_\epsilon)$
PatchTST	$O(\frac{L^2}{P^2} + \frac{Ld}{P})$	$O(\frac{T^2 d_\epsilon}{P^2})$
Informer	$O(Ld \log L)$	$O(Td_\epsilon \log T)$
Autoformer	$O(L^2 + Ld)$	$T^2 d_\epsilon$
Reformer	$O(Ld \log L)$	$O(Td_\epsilon \log T)$
RNN	$O(Ld^2)$	$O(Td_\epsilon^2)$
ESN	$O(N_r^2)$	$O(TN_r^2)$
Echoformer	$O(\frac{L^2}{P^2} + \frac{Ld}{P} + kN_r L)$	$O(\frac{T^2 d_\epsilon}{P^2} + N_r k^2)$

Table 8: Memory and time complexity comparison.

Table 9: Per-epoch Training Efficiency comparison

Models	Training time per Epoch	Parameters	Disk Usages
PatchTST	1.46 min/epoch	85,169	380GB
EchoFormer	3.24 min/epoch	103,720	407GB
TPGN	4.72 min/epoch	3,004,495	550GB

In Table 8, we compare our methods with several other baseline models on the memory (cache) footprint and time complexity of different models, and the notations are as follows. N_r is the **X-ESNs** states output dimension; L is the number of **X-ESNs** in the group **X-ESNs**; k is the short-term context window length; T is the long-term context total input length; ly is the number of layers; H is the number of attention heads; c is the Compressive Transformer memory size; r is the compression ratio; p is the number of soft-prompt summary vectors; v is the summary vector accumulation steps; s is the kernel size; P is the patch size; d_ϵ is the embedding model dimension; d_k is the dimension of keys in attention; and d_v is the dimension of values in attention. The baselines include PatchTST Nie et al. (2023) which reduces sequence length via patches, significantly lowering complexity; Informer Zhou et al. (2021) which uses ProbSparse self-attention, suitable for long sequences; Autoformer Wu et al. (2022) which introduces auto-correlation mechanism, but the attention remains $O(L^2)$; Reformer Kitaev et al. (2020) which uses LSH to reduce attention computation complexity; and RNN model which computes multi-variants time series step-by-step, holding low complexity but struggles with long-range dependencies. Since we use PatchTST as our base-model, the memory complexity and time complexity of **EchoFormer** is $O((T/p)^2 \cdot d_\epsilon + N_r \cdot k^2)$ and $O((T/p)^2 \cdot d_\epsilon + L \cdot T^2)$ which looks similar with other Transformer-based model with additional memory and time required for tracking, computing and using **X-ESNs** states.

The specific training time, GPU usage and efficiency is shown in Table 3, Figure 15 and Figure 9. Although **EchoFormer**’s structure is more complex than PatchTST, our experiments demonstrate its faster convergence rate. While requiring marginally more time per epoch, **EchoFormer** achieves significantly greater loss reduction compared to baseline models (Figure 15). Consequently, despite slightly higher GPU memory requirements, the total training time remains comparable to or shorter than existing approaches.

J VARIABLE DESCRIPTIONS

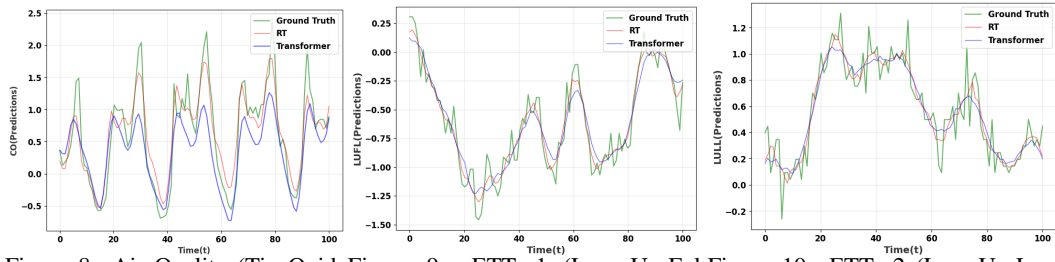
We have described the used variables and math notations in Table 10.

Variable	Description
$M(\cdot)$	Transformer model
$R(\cdot)$	Deep X-ESNs computing
u_t	Input at t time steps
x_t	X-ESNs state at t time steps
y_t	Linear output of X-ESNs
h_t	Embedding of time steps
o_t	Ensembling of group X-ESNs
T	Total time input length
k	Look back window
N_r	X-ESNs size
N_u	X-ESNs input size
m	X-ESNs output size
L	Number of X-ESNs in Group
τ	Forecasting horizons
d_ϵ	Model dimension
d_k	Dimension of key in attention
d_v	Dimension of value in attention
c	Compressive Transformer memory size
r	Compression ratio
p	Number of soft-prompt summary vectors
s	Kernel size
P	Patch size
ϕ_{MLP}	MLP readout layer
W_1 and W_2	learnable diagonal matrices for X-ESNs
Φ	Transformer's learnable parameters
W_q	Queries weights
W_v	Values weights
W_k	Keys weights
W_{in}	Input-to- X-ESNs weight matrix
W	X-ESNs weight matrix
θ	Bias-to- X-ESNs weight
W_{out}	X-ESNs -to-readout weight matrix
θ_{out}	Bias-to-readout weight

Table 10: Descriptions of all variables used in this paper

K X-ESNs SETTINGS

Here we list the **X-ESNs** settings for all 10 different **X-ESNs** in Table6.



Output Examples: Figure 8, Figure 9, and Figure 10 represent examples on the predicted signal versus the original signal. The cyan line is ground truth; the red line is the prediction using RT; and the blue line is the prediction using Transformer as comparison.

L ADDITIONAL COMPONENT ABLATION STUDY

Table 11: Additional Component Ablation Study

Models	MSE	MAE
ESN	0.681	0.657
with MLP readout	0.627	0.606
with Leaky Matrices	0.621	0.598
with Group on sample	0.619	0.592
with Diverse MCRA Function	0.608	0.575
with Embedding σ	0.554	0.527
with Cross-attention combination \cup (EchoSolo)	0.441	0.466
with Basemodel (EchoFormer)	0.368	0.381

M CHAOTIC DATASET: LORENZ EXTRACTOR

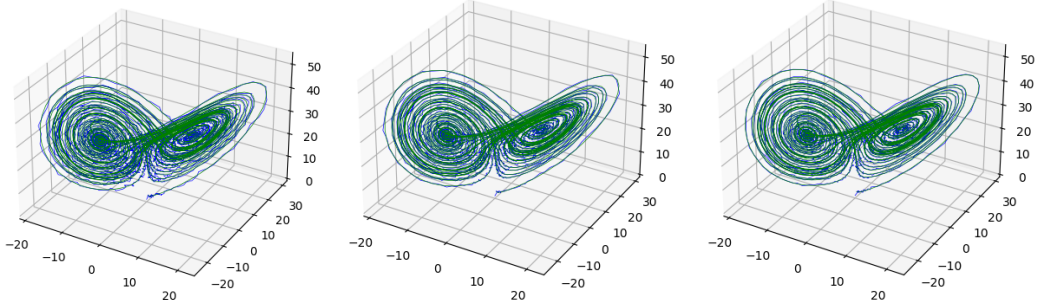


Figure 11: Lorenz with DLinear. Figure 12: Lorenz with PatchTST. Figure 13: Lorenz with **ECHO FLOW NETWORKS**.

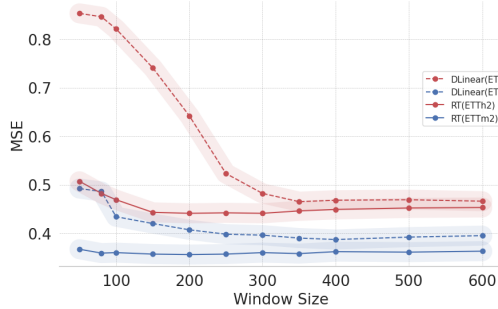


Figure 14: MSE vs. history length.

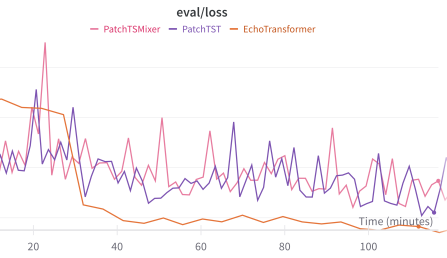


Figure 15: MSE vs. time.